Chemical Engineering Journal 155 (2009) 728–735

Contents lists available at ScienceDirect

Chemical Engineering Journal

journal homepage: www.elsevier.com/locate/cej

Effect of pH on cadmium (II) removal from aqueous solution using titanosilicate ETS-4

Lidiana D. Barreira[a], Patrícia F. Lito[a], Bruno M. Antunes[a], Marta Otero[b], Zhi Lin[a], João Rocha[a], Eduarda Pereira[b], Armando C. Duarte[b], Carlos M. Silva[a,*]

[a] CICECO, Department of Chemistry, University of Aveiro, 3810-193 Aveiro, Portugal
[b] CESAM, Department of Chemistry, University of Aveiro, 3810-193 Aveiro, Portugal

ARTICLE INFO

Article history:
Received 25 May 2009
Received in revised form 6 September 2009
Accepted 7 September 2009

Keywords:
Cadmium
ETS-4
Ion exchange
Batch experiments
Nernst–Planck

ABSTRACT

Cadmium is one of the most toxic contaminants of superficial waters, whose effects are particularly harmful to human health. In 20 years the European Union will impose total elimination of cadmium from industrial discharges. Such facts induce researchers to develop fine separation processes for cadmium removal, especially at the tertiary treatment level.

In this work, we studied the applicability of the microporous titanosilicate ETS-4 (Engelhard Titanium Silicates No. 4) to uptake Cd^{2+} from aqueous solution, in order to evaluate its potential as ion exchanger material. The effect of pH was investigated by performing batch stirred tank experiments. The results obtained shown that Cd^{2+} removal increases up till pH 6, which is a very important conclusion since this value is commonly found in effluents and other wastewaters.

The equilibrium data at pH 6 were accurately represented by the Langmuir–Freundlich isotherm under the experimental conditions studied (average absolute deviation, AAD = 1.67%). The amount of Cd^{2+} removed by ETS-4 at pH 6 clearly surmount results found in literature for the same titanosilicate at pH 4 and for different materials.

The kinetic of Cd^{2+} uptake by ETS-4 was analyzed using a Nernst–Planck based model. The absolute average deviation found point out the reasonable data representation accomplished by Nernst–Planck: AAD = 17.2%.

© 2009 Elsevier B.V. All rights reserved.

1. Introduction

Cadmium is a toxic contaminant extremely harmful to the human health. The presence of cadmium in the environmental is mainly due to effluents discharged by several industries, including metal plating, cadmium–nickel batteries, petroleum refining, mining, pigments, stabilizers, alloys, agriculture, and electronics [1,2]. The bioaccumulation of cadmium and other metallic pollutants together with their associated hazardous effects, mainly when present in drinking waters, is of great concern and has led to development of increasingly strict environmental regulations. For instance, in the European Union the maximum permissible concentration of total cadmium for drinking water is 5 $\mu g\,L^{-1}$ [3]. The effluent discharge limit in Portugal is 0.2 $mg\,L^{-1}$ [4]. Moreover, the Water Framework Directive (2000/60/EC) will impose total elimination of cadmium from industrial discharges in 20 years. Therefore, the development of clean-up technologies for removing cadmium from wastewaters and remediation of polluted ecosystems are of special importance.

The removal of toxic metals from wastewaters can be carried out by a number of separation technologies, such as chemical precipitation, membrane processes, ion exchange, adsorption, and solvent extraction [5]. Nonetheless, many of those conventional technologies may be inadequate, expensive or produce large amounts of sludge, which create disposal difficulties [6,7]. Moreover, they are usually not able to reduce economically toxic metal concentration to extremely low levels as required by environmental regulations, which limits its application in purification of drinking waters. For instance, chemical precipitation, mostly used to separate metal ions from solution, has played a major role in water treatment for a long time, being widely used for the treatment of many wastewaters before discharge [8]. Nonetheless, the removal of small trace compounds and high removal efficiencies usually imply the formation of a carrier precipitate to incorporate or adsorb the contaminant. Unfortunately, the waste volume from carrier precipitation may be considerable even for trace concentrations, which induces researchers to select alternative processes such as adsorption and ion exchange. These methods are most effective with dilute

* Corresponding author at: Department of Chemistry, University of Aveiro, Campus Universitário de Santiago, 3810-193 Aveiro, Portugal. Tel.: +351 234 401549; fax: +351 234 370084.
E-mail address: carlos.manuel@ua.pt (C.M. Silva).

1385-8947/$ – see front matter © 2009 Elsevier B.V. All rights reserved.
doi:10.1016/j.cej.2009.09.014

Nomenclature

AAD	average absolute deviation
A^{z_A}	generic counter ion A^{z_A} in solution
$\overline{A^{z_A}}$	generic counter ion A^{z_A} in the exchanger
B^{z_B}	generic counter ion B^{z_B} in solution
$\overline{B^{z_B}}$	generic counter ion B^{z_B} in the exchanger
C_A	concentration of A in bulk solution (mol m^{-3})
d_p	particle diameter (m)
D_{Aw}	diffusivity of species A in solution (m^2 s^{-1})
D_A, D_B	self-diffusion coefficient of species A and B (m^2 s^{-1})
D_{AB}	interdiffusion coefficient of the pair A–B (m^2 s^{-1})
F	Faraday constant (C mol^{-1})
k_f	convective mass transfer coefficient (m s^{-1})
K_F	Freundlich parameter
K_L	Langmuir parameter
K_{LF}	Langmuir–Freundlich parameter
mETS-4	mass of ETS-4 (kg)
n_F	Freundlich parameter
n_{LF}	Langmuir–Freundlich parameter
N_A, N_B	intraparticle molar flux of species A and B (mol(m^2 s)$^{-1}$)
Q	ion exchanger capacity (mol m^{-3})
q_A, q_B	molar concentration of counter ions A and B in the particle (mol m^{-3})
$\bar{q}_A$	average concentration of counter ion A in the particle (mol m^{-3})
$q_{max,L}$	maximum ion exchanger capacity in the Langmuir isotherm (eq m^{-3})
$q_{max,LF}$	maximum ion exchanger capacity in the Freundlich isotherm (eq m^{-3})
r	radial position in the particle (m)
R	particle radius, m; % of ion removed relative to the excess over final equilibrium concentration
$\Re$	gas constant (J/mol K^{-1})
Re	$= \varepsilon^{1/3} d^{4/3}/\nu$, Reynolds number
Sc	$= \nu/D$, Schmidt number
Sh	$= k_f d/D$, Sherwood number
T	temperature (K)
t	time (s) (and h in figures)
t_{st}	stoichiometric time (s)
V_L	volume of solution (m^3)
V_{ETS-4}	volume of ETS-4 (m^3)
Z_A, Z_B	charges of components A and B

Greek letters

ε	bed porosity; mixer power input per unit of fluid mass (m^2 s^{-3})
ϕ	electric potential (V)
ρ_{ETS-4}	density of ETS-4
τ	space-time (s)
ν	kinematic viscosity (m^2 s^{-1})

Subscripts

0	initial condition
A	counter ion initially present in solution (Cd^{2+})
B	counter ion initially present in particle (Na^+)
eq	equilibrium
F	Freundlich
f	feed condition
L	Langmuir
LF	Langmuir–Freundlich
NP	Nernst–Planck
s	solid–liquid interface

solutions and can reduce concentrations many-fold, being attractive as polishing steps after former approaches to remove the bulk of the contaminant. At the end, the sorbents containing considerable metal loadings may be destroyed or sent to landfills and grouts (when release is sufficiently slow) or regenerated. However, the cost of sorbents and its possible regeneration are important limiting factors for the applicability of these methods [5].

Natural and synthetic zeolites are gaining considerable interest because of their high selectivity and ion exchange capacity [9,10]. However, sorption data of synthetic zeolites are more reproducible and interpretable because of their higher phase purity.

Microporous titanosilicates are three-dimensional crystalline solids with a well defined structure containing titanium, silicon and oxygen atoms [11]. These materials have a regular crystalline framework formed by a three-dimensional combination of tetrahedral and octahedral building blocks connected with each other by shared oxygen atoms. Each TiO_6 octahedron in the titanosilicate global structure carries a −2 charge, which can be neutralized by extra-framework cations (usually Na^+ and K^+). These compensation species, as well as water molecules or other adsorbed molecules, are located in the channels of the structure and can be replaced by others. Like zeolites, titanosilicates exhibit remarkable physical and chemical properties, such as selective sorption, ion exchange and catalytic activity [11]; in addition, the framework anionic sites are typically divalent, which should be particularly useful for the exchange of divalent ions. Of special importance for environmental uses is their ability to uptake and retain toxic metal species from aqueous media, such as Hg^{2+} and Cd^{2+}. ETS-4 contains octahedral and square-pyramidal titanium units, in addition to the tetrahedral silicate units. The 12-ring channels are separated by the 8-ring windows. ETS-4 has been suggested as good ion exchanger [11].

A number of titanosilicates have recently been used as ion exchangers for toxic metals removal. For instance, Bortun et al. [12] evaluated framework and layered titanosilicates for cesium and strontium uptake from contaminated groundwater and wastewater; Decaillon et al. [13] studied the ion exchange selectivity of layered titanosilicate AM-4 toward strontium; Koudsi and Dyer [14] studied a synthetic titanosilicate analog of the mineral penkvilsite-2O, i.e. AM-3, for removal of cobalt-60; Lopes et al. [15–17] evaluated the potential of synthetic microporous (ETS-4, ETS-10, and AM-2) and layered (AM-4) titanosilicates for decontamination of natural waters polluted with low mercury levels; Ferreira et al. [18] investigated the ability of ETS-4 to uptake Cd^{2+} from aqueous solution, and Popa et al. [19] studied its ability to remove $^{60}Co^{2+}$, $^{115m}Cd^{2+}$ and $^{203}Hg^{2+}$ radiocations from their aqueous solutions. Moreover, ETS-10 has been shown to have high selectivity for several toxic metals such as Pb^{2+}, Cu^{2+}, Cd^{2+}, Co^{2+}, Mn^{2+}, Zn^{2+} [20,21]. The results obtained have revealed the high potential of titanosilicates as decontaminant agents.

In this work, we studied the applicability of the titanosilicate ETS-4 to uptake Cd^{2+} from aqueous solution, in order to evaluate its potential as tertiary treatment of industrial effluents. This study is carried out here with crystal in powder form to judge and predict its future application in supported pellets. Batch experiments were carried out, and the effect of pH was carefully analyzed in the range 4–8. Modelling was accomplished using a Nernst–Planck based model [22–24].

2. Experimental

2.1. Materials and solutions

All glassware used in the experiments was immersed in concentrated nitric acid during 12 h, then in nitric acid 25% during 12 h, and finally washed with ultrapure Milli-Q water prior to use.

Table 1
Features of the ETS-4 particles used [25].

Formula	$[(Na,K)_2TiSi_{2.5}O_{13}{\cdot}4H_2O]$
Density ($kg\,m^{-3}$)	2200
Ion exchanger capacity ($eq\,kg^{-1}$)	6.39
Particle diameter (10^{-6} m)	0.5–0.9
Pore diameter (10^{-10} m)	3–4

Chemicals used were of analytical reagent grade and obtained from chemical commercial suppliers (Merck), without further purification. The certified standard stock solution of cadmium nitrate ($1001 \pm 2\,mg\,L^{-1}$) was purchased from Merck.

Cd^{2+} solutions were prepared daily by diluting the stock solution to the desired concentration in high purity water (18 MΩ cm). The stock solution of cadmium nitrate is extremely acidic and when it is diluted in 2 L of water, solutions with pH values around 4 are obtained. NaOH was added to these solutions in order to fix them in different pH. The pH remains approximately constant (±0.1) during the experiments even with no buffer solution added.

ETS-4 was used as cation exchanger to remove Cd^{2+} ions. The synthesis of ETS-4 was performed as follows: an alkaline solution was made by dissolving 33.16 g of metasilicate (BDH), 2.00 g NaOH (Merck), and 3.00 g KCl (Merck) into 25.40 g H_2O. 31.88 g of $TiCl_3$ (15%, w/w, $TiCl_3$ and 10%, w/w, HCl, Merck) were added to this solution and stirred thoroughly. This gel, with a molar composition 5.9 Na_2O:0.7 K_2O:5.0 SiO_2:1.0 TiO_2:114 H_2O, was transferred to a Teflon-lined autoclave and treated at 230 °C for 17 h under autogenous pressure without agitation. The product was filtered off, washed at room temperature with distilled water, and dried at 70 °C overnight, the final product being an off-white microcrystalline powder. Table 1 summarises most important features of ETS-4.

The powder X-ray pattern was recorded on a Philips X'Pert MPD diffractometer using CuKα X-radiation. The morphology and crystal size of the samples were examined using scanning electron microscope (SEM) on a Hitachi S-4100 microscope.

2.2. Batch experiments

All experiments were carried out in batch isothermal (295 ± 1 K) conditions in a closed volumetric flask ($2 \times 10^{-3}\,m^3$) to avoid evaporation. In such a vessel, for each experiment, a known mass of ETS-4 was added to a Cd^{2+} aqueous solution with an initial concentration of $0.85 \times 10^{-3}\,kg\,m^{-3}$ and this time was considered the starting point of the experiment. The experimental conditions may be found in Table 2.

Table 2
Experimental conditions studied (temperature: $T = 295 \pm 1$ K; solution volume: $V_L = 2 \times 10^{-3} m^3$; initial Cd^{2+} concentration: $C_{A,0} = 0.85 \times 10^{-3}\,kg\,m^{-3}$).

Experiment	pH	Data measured	Mass of ETS-4, 10^{-6} kg
1	4	Kinetic and equilibrium	25.2
2			50.3
3	6	Kinetic and equilibrium	4.3
4			25.0
5			50.3
6	6	Equilibrium	1.5
7			2.5
8			7.5
9			10.0
10			15.0
11			5.0
12	8	Kinetic and equilibrium	25.1
13			50.1

ETS-4 particles and Cd^{2+} aqueous solutions were maintained in contact under constant stirring until Cd^{2+} concentration remained constant. Several aliquots (10 mL) filtered through a 0.45 μm Acetate Plus Osmonics filter were taken from the vessel along time. The filtrate was adjusted to pH < 2 with HCl, stored at 277.15 K, and then analysed by inductively coupled plasma mass spectrometry [26] on a Thermo ICP-MS X Series equipped with a Burgener nebuliser. A blank experiment (without ETS-4) was always run as a control, to check that the removal of Cd^{2+} occurred by ion exchange onto ETS-4 and not by adsorption on the vessel walls, for instance.

Two experiments were accomplished at pH 4 (Exps. 1 and 2) and another two at pH 8 (Exps. 12 and 13), from which four kinetic curves were determined. At pH 6 nine experiments were performed: Exps. 3–5 gave rise to kinetic curves, whereas Exps. 6–11 were only carried out to measure additional equilibrium points for the isotherm.

The average concentration of sorbed metal at time t, $\bar{q}_A$, was calculated by material balance:

$$\bar{q}_A = \frac{\left(C_{A,0} - C_A\right) V_L}{V_{ETS\text{-}4}} \tag{1}$$

where subscript 'A' denotes Cd^{2+}, $C_{A,0}$ is the initial solution concentration, C_A is the solution concentration at time t, V_L is the solution volume, $V_{ETS\text{-}4} = m_{ETS\text{-}4}/\rho_{ETS\text{-}4}$ is the volume of titanosilicate, m is the mass of ETS-4, and $\rho_{ETS\text{-}4}$ is its density. Furthermore, the percentage of Cd^{2+} removed relative to the excess over final equilibrium concentration ($C_A - C_{A,eq}$) was also determined:

$$R = \frac{C_{A,0} - C_A}{C_{A,0} - C_{A,eq}} \times 100 \tag{2}$$

3. Modelling

The NP model adopted in this work to describe the batch ion exchange has been already presented in detail in a previous publication [16] dealing with Hg^{2+} removal from aqueous solution using ETS-4. It embodies the following hypothesis: (i) film and intraparticle mass transfer resistances; (ii) spherical solid particles; (iii) perfectly stirred tank; (iv) isothermal operation; (v) liquid and solid volume changes are neglected; (vi) co-ions are excluded from the particles (Donnan exclusion); (vii) ideal solution behaviour.

3.1. Kinetic curves and isotherms

Ion exchange may be represented by conventional chemical equilibrium [22]. For the case where the titanosilicate is initially in B (Na^+) form and the counter ion in solution is A (Cd^{2+}), the equilibrium may be represented by:

$$z_A \overline{B^{z_B}} + z_B A^{z_A} \Leftrightarrow z_B \overline{A^{z_A}} + z_A B^{z_B} \tag{3}$$

where Z_A and Z_B are the electrochemical valences.

In dilute ionic solutions, intraparticle flux of each counter ion can be accurately described by the Nernst–Planck equations [22]:

$$N_A = -D_A \nabla q_A - D_A z_A q_A \frac{F}{\Re T} \nabla \phi \quad \text{and}$$

$$N_B = -D_B \nabla q_B - D_B z_B q_B \frac{F}{\Re T} \nabla \phi \tag{4}$$

where D_A and D_B are the self-diffusion coefficients of A and B, respectively, q_A and q_B are the molar concentrations of A and B in the particle, F is Faraday constant, $\Re$ is gas constant, T is absolute temperature, ϕ is the electric potential, and ∇ is the gradient operator.

In the development of the model equations, the system is assumed to be subjected to the conditions of electroneutrality and

nonexistent electric current:

$$q_A z_A + q_B z_B = Q \quad \text{and} \quad z_A N_A + z_B N_B = 0, \tag{5}$$

where Q is the ion exchanger capacity. The resulting Nernst–Planck equations are presented here as a special form of Fick's first law, in non-dimensional form, where a coupled interdiffusion coefficient, D^*_{AB}, appears:

$$N^*_A = -D^*_{AB}\left(\frac{\partial y_A}{\partial \xi}\right), \text{ with } \quad D^*_{AB} = \frac{\delta(z_A y_A + z_B y_B)}{z_A y_A + \delta z_B y_B} \tag{6}$$

Non-dimensional variables are defined as follows:

$$\delta = \frac{D_B}{D_A}, \quad y_A = \frac{z_A q_A}{Q}, \qquad \xi = \frac{r}{R}, \quad N^*_A = \frac{z_A R}{Q D_A} N_A \tag{7}$$

where R is the particle radius and r is the radial coordinate.

The material balances in the particle and in the vessel, together with the corresponding initial and boundary conditions, are compiled in Table 3.

With respect to the equilibrium representation, the Freundlich, Langmuir and the Langmuir–Freundlich isotherms have been examined in this work (Eqs. (8)–(10) in Table 3). Accordingly, K_F and n_F are the parameters of the Freundlich isotherm, K_L and $q_{max,L}$ are the Langmuir parameters, and $q_{max,LF}$, $1/n_{LF}$ and K_{LF} are the Langmuir–Freundlich parameters. Moreover, $q_{A,eq}$ is the equilibrium concentration of counter ion A in the particle (eq m^{-3}).

The simultaneous solution of the NP equations gives the concentration of the Cd^{2+} in solution, and its concentration profiles in the solid phase as function of time. The model has been solved numerically using the Method of Lines [27] and integrated using the Finite-Difference approach. For this purpose, a programme in Matlab has been written to solve the resulting Ordinary Differential Equations (ODEs) with 101 grid points. An odd number of grid points are required when the average loading (Eq. (13)) is numerically evaluated using the 1/3 Simpson's Rule. Ode15s solver has been used to integrate this set of ODEs of the initial-value type.

With respect to the solution approach, a first optimisation step was performed based on the 'elimination of linear parameters in nonlinear regression' technique due to Lawton and Sylvestre [28]. With this procedure, one reduces the number of parameters that must be estimated and fasts the convergence. Thus, only two initial guesses have to be provided instead of three: specifically the diffusivities ratio, D_A/D_B, and k_f. Finally, an enhancing global optimisation involving all parameters simultaneously was performed, where the previous results were taken as reliable initial guesses.

For well established agitated systems, k_f may be predicted using correlations which depend generally on the Reynolds, Schmidt and Power numbers, and on geometrical parameters such as the ratio of impeller to tank diameter, the specific geometry of the impeller, and the geometry of baffling, if any, used to inhibit vortex formation in the vessel. For the particular geometry of our sorption set-up no correlation is available in the literature. Nonetheless, the correlation of Armenante and Kirwan [29] has been adopted to estimate the convective mass transfer coefficient at least to predict its order of magnitude:

$$Sh = 2 + 0.52\, Re^{0.52} Sc^{1/3} \tag{18}$$

where $Sh = k_f d_p / D_{Aw}$ is the Sherwood number, d_p is the particle diameter, D_{Aw} is the diffusivity of the solute in solution, $Re = \varepsilon^{1/3} d_p^{4/3}/\nu$ is the Reynolds number, ε is the mixer power input per unit of fluid mass, ν is the kinematic viscosity, and $Sc = \nu/D_{Aw}$ is the Schmidt number. This equation is frequently applied to fix k_f in the model equations or, alternatively, to estimate k_f and compare it with the optimized value from experimental data [30,31].

3.2. Performance of an ion exchange bed

In order to produce a nearly contaminant-free effluent, ion exchange and adsorption are usually carried out in percolation columns packed with solid sorbents. The feed stream is fed constantly to the bed, and the treated fluid exits the other end of the column until equilibration is approached. The large ion exchange capacity of ETS-4 leads us to estimate the ratio between stoichiometric time (t_{st}) and space-time (τ) of a percolation column, which is an essential parameter for equipment design [32]:

$$t_{st} = \tau\left(1 + \frac{1-\varepsilon}{\varepsilon}\frac{q_{A,eq,f}}{C_{A,f}}\right) \tag{19}$$

Here, $q_{A,eq,f}$ is titanosilicate loading in equilibrium with feed concentration $C_{A,f}$, and ε is bed porosity. The stoichiometric time corresponds to the time needed for a shock wave front to cross the column, which occurs with favourable isotherms (i.e., concavity downward) and beds ideally in equilibrium with the feed, i.e. the fluid and solid concentration profiles are uniform.

Table 3
Mathematical models equations.

Freundlich isotherm	$q_{A,eq} = K_F C_{A,eq}^{1/n_F}$	(8)
Langmuir isotherm	$q_{A,eq} = \dfrac{q_{max,L} K_L C_{A,eq}}{1 + K_L C_{A,eq}}$	(9)
Langmuir–Freundlich isotherm	$q_{A,eq} = \dfrac{q_{max,LF} K_{LF} C_{A,eq}^{1/n}}{1 + K_{LF} C_{A,eq}^{1/n}}$	(10)
Material balances	$\left(\dfrac{\partial q_A}{\partial t}\right) = -\dfrac{1}{r^2}\dfrac{\partial}{\partial r}(r^2 N_A)$	(11)
	$\dfrac{\partial C_A}{\partial t} = -\dfrac{V_{ETS\text{-}4}}{V_L}\dfrac{\partial \bar{q}_A}{\partial t}$	(12)
	$\bar{q}_A = \dfrac{3}{R^3}\displaystyle\int_0^R r^2 q_A dr$	(13)
Initial and boundary conditions	$t = 0, \quad \begin{cases} q_A = \bar{q}_A = 0 \\ C_A = C_{A,0} \end{cases}$	(14)
	$r = R, \quad q_A = q_{A,R}$	(15)
	$r = 0, \quad \left(\dfrac{\partial q_A}{\partial r}\right) = 0$	(16)
Equality of internal and film ionic fluxes	$\left(\dfrac{\partial q_A}{\partial r}\right)_{r=R} = \dfrac{k_f}{D_{AB}}(C_A - C_{As})$	(17)

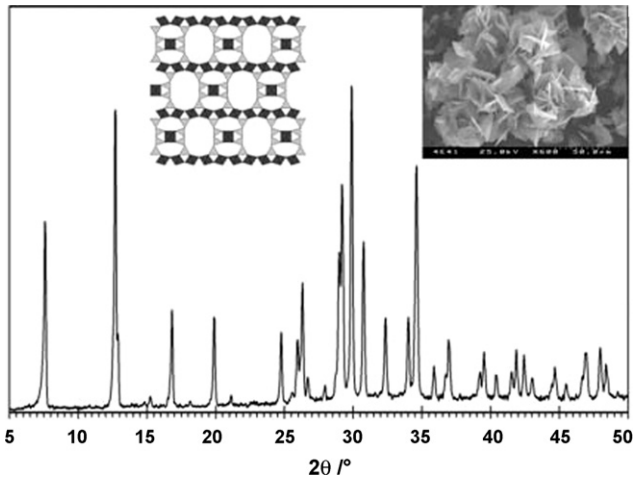

Fig. 1. Powder XRD, SEM image and structure representation of ETS-4 materials.

4. Results and discussion

The powder XRD pattern of the sample used in this work is shown in Fig. 1, which is identical to that of ETS-4 materials reported in the literature, indicating that the samples used in this experiment are highly pure ETS-4. SEM image of the sample (right inset in Fig. 1) displays a plate shape of ETS-4 crystals with a thickness of *ca.* 1 μm, also confirming that this is a pure ETS-4 sample. The left inset in Fig. 1 is the structure representation of ETS-4, showing the 12- and 7-membered ring.

Figs. 2–4 show the batch experiments results, expressed in $C_A/C_{A,0}$ *versus t* form, for different pH values (pH 4, 6 and 8) and titanosilicate masses (see experimental conditions in Table 2). As can be observed, the trends found are similar, showing a fast initial uptake followed by the characteristic slower removal towards the equilibrium. Such behavior is due to the large driving force for ions transport at beginning of the process, since ETS-4 particles are initially free of Cd^{2+}. It is also evident that the Cd^{2+} removal increases by increasing ETS-4 mass, because the extensive ion exchange capacity is proportional to the titanosilicate mass.

The results obtained at distinct pH (Figs. 3 and 4) evidence that metal uptake is more effective when pH is increased up till 6. As

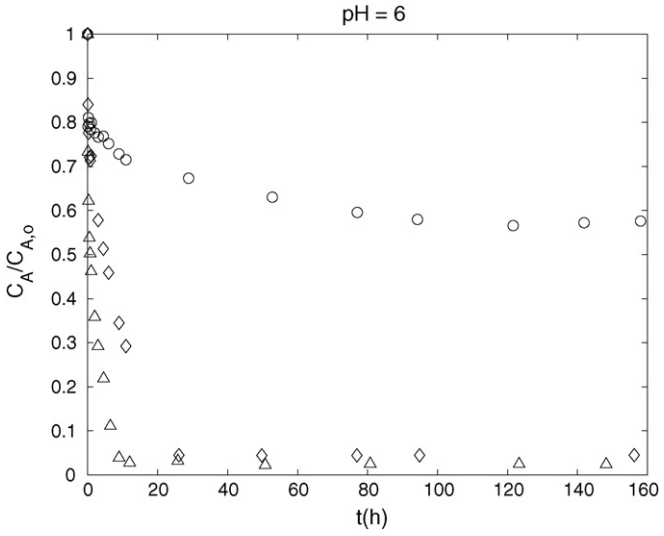

Fig. 2. Normalized concentration of bulk solution *versus* time at pH 6. Experimental conditions (see Table 2): Symbols: (○), Exp. 3 (pH 6, m = 4.3 mg); (◊), Exp. 4 (pH 6, m = 25.0 mg); (△), Exp. 5 (pH 6, m = 50.3 mg).

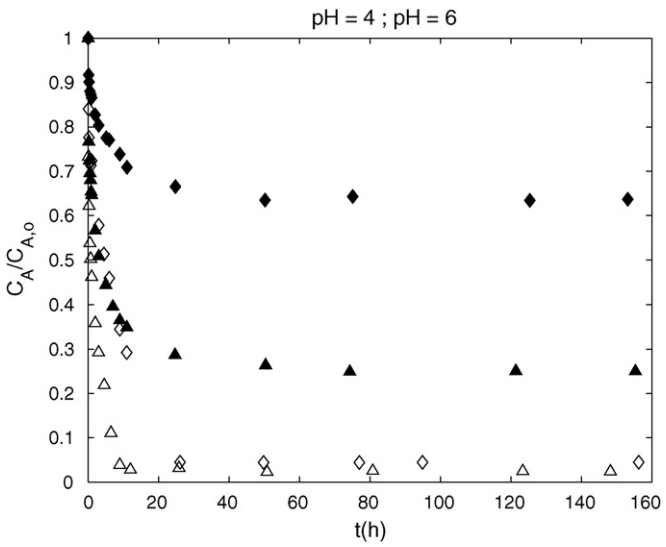

Fig. 3. Effect of pH on the normalized concentration of bulk solution *versus* time (pH 4 and pH 6). Experimental conditions (see Table 2): Symbols: (♦), Exp. 1 (pH 4, m = 25.2 mg); (▲), Exp. 2 (pH 4, m = 50.3 mg); (◊), Exp. 4 (pH 6, m = 25.0 mg); (△), Exp. 5 (pH 6, m = 50.3 mg).

seen in Fig. 3, when pH goes from 4 to 6, Cd^{2+} uptake increases significantly: for m = 25 mg, $C_{A,eq}/C_{A,0}$ = 0.64 at pH 4, while it drops only to 0.04 at pH 6; for m = 50 mg, the two values found are 0.25 and 0.02, respectively. This behavior is attributed to the competition between H^+ and Cd^{2+} ions to the titanosilicate sorption sites at lower pH values, given the higher concentration of H^+ in solution. When pH is increased from 6 to 8 (Fig. 4) the removal enhancement is almost insignificant. These results reveal the importance of pH in the process, and show the ion exchange efficiency is highest around pH 6. This has great impact in practice, since pH of wastewaters and several industrial effluents is around 6, which avoids the inclusion of any previous pH control. Hence, in this work we focused on the determination of the isotherm of the system Cd^{2+}/H_2O/ETS-4 at pH 6.

The effect of pH on the removal of different metal ions has been investigated using several ion exchangers, and similar results have

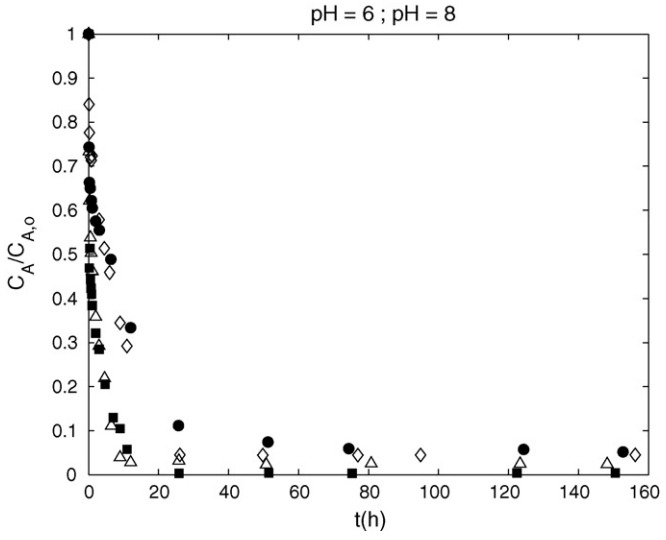

Fig. 4. Effect of pH on the normalized concentration of bulk solution *versus* time (pH 6 and pH 8). Experimental conditions (see Table 2): Symbols: (◊), Exp. 4 (pH 6, m = 25.0 mg); (△), Exp. 5 (pH 6, m = 50.3 mg); (●), Exp. 12 (pH 8, m = 25.1 mg); (■), Exp. 13 (pH 8, m = 50.1 mg).

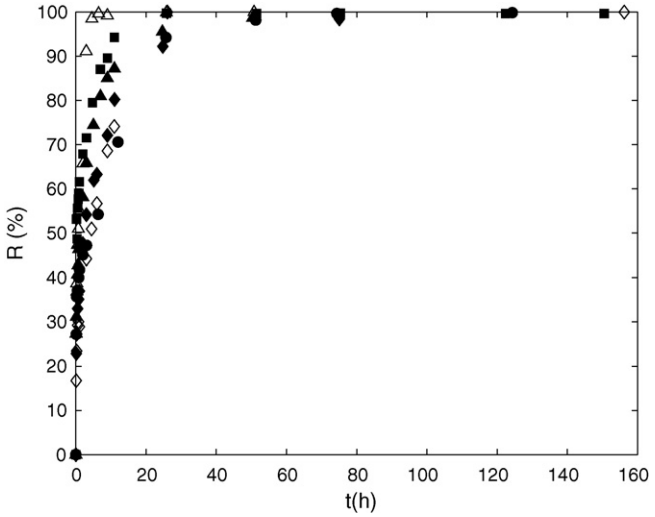

Fig. 5. Percentage of Cd^{2+} removed relative to the excess over final equilibrium concentration as a function of time. Experimental conditions (see Table 2): Symbols: (♦), Exp. 1 (pH 4, m = 25.2 mg); (▲), Exp. 2 (pH 4, m = 50.3 mg); (○), Exp. 4 (pH 6, m = 25.0 mg); (△), Exp. 5 (pH 6, m = 50.3 mg); (●), Exp. 12 (pH 8, m = 25.1 mg); (■), Exp. 13 (pH 8, m = 50.1 mg).

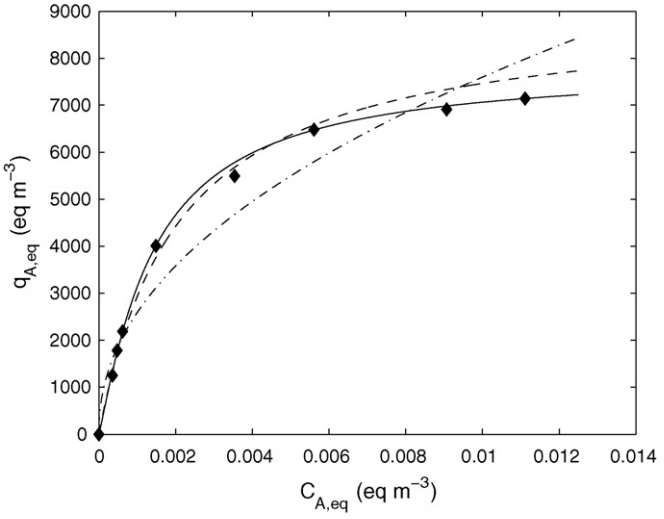

Fig. 6. Equilibrium data at pH 6 along with Freundlich, Langmuir and Langmuir–Freundlich isotherms fitted (T = 295 K). Symbols (lozenges): experimental data; dashed line: Langmuir isotherm; dash-dotted line: Freundlich isotherm; solid line: Langmuir–Freundlich isotherm.

been obtained by other researchers. For instance, Lv et al. [20] have observed such a sharp increase for Cd^{2+} and Cu^{2+} on ETS-10, increasing pH from 2.5 to 6. Mishra et al. [33] carried out the uptake of Cd^{2+} on alkali metal titanates, and observed a significant reduction of the sorbed amount by decreasing pH from 10.2 to 3.1. Kocaoba [34] showed that the Cd^{2+} and Pb^{2+} exchange on Amberlite IR 120 resin and dolomite increased when pH goes from 1 to 8. Similar results were also obtained by El-Kamash [35] for Cs^{+} and Sr^{2+} removal on zeolite A.

The percentage of Cd^{2+} removed relative to the excess over final equilibrium concentration (see Eq. (2)) is represented in Fig. 5. Results obtained under the same pH conditions confirm that for larger masses of titanosilicate the uptake is faster and the sorbed quantities are superior. For instance, at pH 6, R = 99.7% is obtained after approximately 26 h using 25.0×10^{-6} kg of ETS-4, while 12 h are sufficient to get R = 99.6% when 50.3×10^{-6} kg of solid is used. It is interesting to compare this equilibration time with that found elsewhere for titanosilicate ETS-10, 1–2 h [36]. Such results are due to the pore diameters of these materials, specifically 0.49 × 0.76 nm (ETS-10) and 0.3–0.4 nm (ETS-4). Since ETS-10 pores are wider, cadmium (II) is expected to diffuse faster through the solid matrix.

Equilibrium data obtained at pH 6 are plotted in Fig. 6, along with the correlations achieved by different isotherms models. The corresponding parameters and absolute average deviations (AAD) are listed in Table 4. From the kinetic curves measured (Exps. 3–5 in Table 2 and Fig. 2) three equilibrium points were calculated by averaging the horizontal branch of those curves. As has been mentioned in Section 2, six additional equilibrium experiments were performed in order to obtain more isotherm points (Exps. 6–11 in Table 2). Fig. 6 and the calculated results reveals the much better performance of Langmuir–Freundlich isotherm to represent our equilibrium data, confirmed by the smaller AAD obtained in comparison to those of Langmuir and Freundlich: AAD_{LF} = 1.67% against AAD_{L} = 5.15% and AAD_{F} = 12.94%, respectively.

Fig. 7 establishes a comparison between our equilibrium data at pH 6 and those available in literature for Cd^{2+} removal using the same titanosilicate and other materials: Ferreira et al. [18] studied the performance of ETS-4 at pH 4.0 and 295 K; Kocaoba [34] analyzed dolomite at pH 5 and 293 K; Sprynskyy et al. [37] used clinoptilolite under pH 6.2, at room temperature; Naiya et al. [38] used a clarified sludge at pH 5.0 and 303 K; and Álvarez-Ayuso and García-Sánchez [39] published data on palygorskite (pH 6.0–7.0 and T = 295 K). It is once more evident from this figure the notorious increase of the sorbed amount of Cd^{2+} when pH is raised from 4 to 6. Besides, it can be observed that the Cd^{2+} removal by ETS-4 significantly surmounts that obtained by the remaining materials, which supports the potential of this titanosilicate for cadmium decontamination. This conclusion is also observed at pH 4.

With respect to ion exchange kinetic modeling, the Cd^{2+} sorption by ETS-4 was studied using a model based on NP equations. In Fig. 8 the NP results for the experiments of Fig. 2 (pH 6) are shown graphically along with data; the corresponding parameters and AAD are compiled in Table 5.

According to Fig. 8, NP represents data fairly well (AAD = 17.2%), except for Exp. 3. The optimized self-diffusion coefficients of Cd^{2+} and Na^{+} were 4.548×10^{-19} and 5.246×10^{-18} m^2 s^{-1}, respectively, which evidence the higher mobility of sodium ions inside particle. The magnitude of those diffusivities is in good agreement with the small pore diameter of ETS-4, i.e. (3–4) × 10^{-10} m and follows other results from literature. For instance, Lopes et al. [16] found diffusivities of 1.108×10^{-19} and 7.873×10^{-19} m^2 s^{-1} for Hg^{2+} and Na^{+} in ETS-4, respectively, and Ferreira et al. [18] obtained 3.204×10^{-19} and 3.195×10^{-18} m^2 s^{-1} for Cd^{2+} and Na^{+} on the same microporous titanosilicate at pH 4. The convective mass transfer coefficient fitted was $k_f = 1.28 \times 10^{-3}$ m s^{-1}, while that predicted by Armenante and Kirwan's correlation was 2.20×10^{-3} m s^{-1}.

Table 4
Langmuir and Langmuir–Freundlich isotherm parameters for pH 6 and average absolute deviations (T = 295 K).

Freundlich isotherm			
K_F (eq m^{-3})$^{1-1/n}$		$1/n_F$	AAD (%)
65447.27		0.47	12.94
Langmuir isotherm			
K_L (m^3 eq^{-1})	$q_{max,L}$ (eq m^{-3})		AAD (%)
480.71	9017.13		5.15
Langmuir–Freundlich isotherm			
K_{LF} (eq m^{-3})$^{1-1/n}$	$q_{max,LF}$ (eq m^{-3})	$1/n_{LF}$	AAD (%)
1771.00	7827.70	1.14	1.67

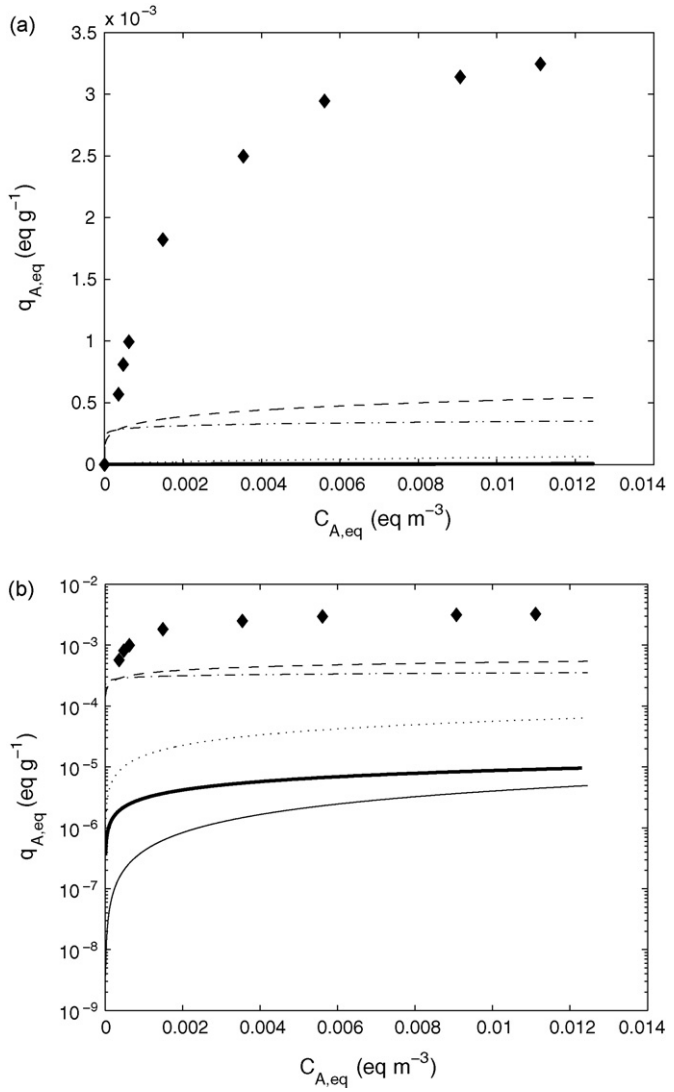

Fig. 7. Comparison between equilibrium data measured in this work (ETS-4, pH 6 and T = 295 K; lozenges) and other isotherms available in literature for ETS-4 and for different solid materials: dashed line: ETS-4 (pH 4.0 and T = 298 K) [18]; dash-dotted line: dolomite (pH 5 and T = 293 K) [34]; dotted line: clarified sludge (pH 5.0 and T = 303 K) [38]; thick solid line: clinoptilolite (pH 6.2 and room temperature) [37]; solid line: palygorskite (pH 6.0–7.0 and T = 295 K) [39] (a) linear scale, (b) log scale.

Such result validates our optimized value, even though some values used in the correlation were not entirely appropriate, namely: (i) the power was approximately calculated, and (ii) the size of our ETS-4 particles ($d = 0.7 \times 10^{-6}$ m) is lower than the inferior limit studied by Armenante and Kirwan [29] (range of d: $(6–420) \times 10^{-6}$ m).

In Fig. 9 the ratio t_{st}/τ for the concentration range of our isotherm (Fig. 6) was calculated by Eq. (4), assuming $\varepsilon \approx 0.5$. As expected, extremely high values (in the range 10^6–10^7) are obtained for our experimental conditions, which means that the concentration wave front moves through the bed at a velocity that is much lower than the interstitial fluid velocity. Furthermore, since our isotherm is

Table 5
Calculated results for the models studied in this work.

Nernst–Planck based model			
D_A ($m^2 s^{-1}$)	D_B ($m^2 s^{-1}$)	k_f ($m s^{-1}$)	AAD (%)
4.548×10^{-19}	5.246×10^{-18}	1.281×10^{-3}	17.2

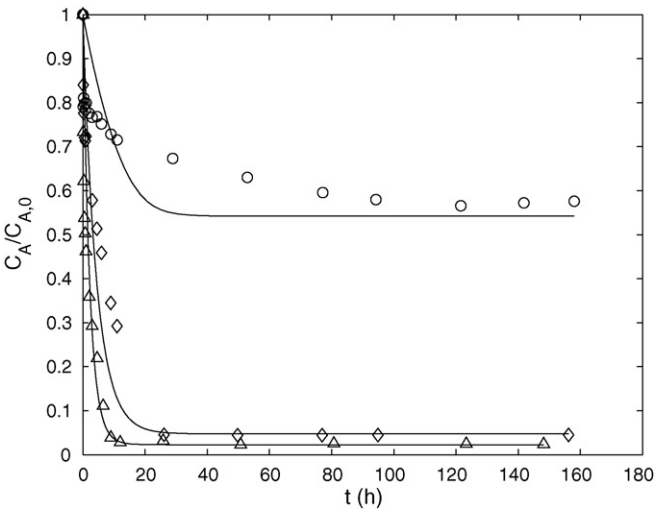

Fig. 8. Normalised concentration of bulk solution *versus* time: NP based model results. Experimental conditions (see Table 2): Symbols: (○), Exp. 3 (pH 6, m = 4.3 mg); (◊), Exp. 4 (pH 6, m = 25.0 mg); (△), Exp. 5 (pH 6, m = 50.3 mg).

of the favourable type, a self-sharpening wavefront arises; hence desirable constant pattern flow develops along bed during loading step. Besides, it can be observed that t_{st}/τ values at pH 6 are one order of magnitude higher than those at pH 4, which evidence again the importance of pH. Furthermore, the results for ETS-4 at pH 4 even surmounts significantly those obtained by the remaining materials; for instance, t_{st}/τ in de range of 10^1–10^2 and $t_{st}/\tau = 2$ were obtained for clinoptilolite and palygorskite, respectively. Accordingly, the technical interest of ETS-4 for commercial applications is once more emphasized. Such results indicate that the synthesis of pellets supporting ETS-4 should be an appealing and promising objective. Concerning ETS-4 regeneration, previous studies showed it can be successfully regenerated with $NaNO_3$ (10^{-3} M).

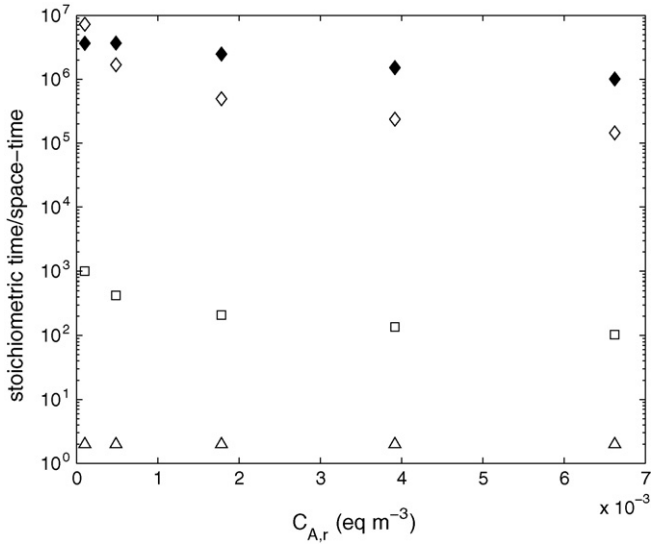

Fig. 9. Ratio between stoichiometric time and space-time plotted for each concentration of the isotherm measured in this work (ETS-4, pH 6 and T = 295 K; lozenges, data in Fig. 5) and other isotherms available in literature for ETS-4 and for different solid materials: (◊), ETS-4 (pH 4.0 and T = 295 K) [18]; (□), clinoptilolite (pH 6.2 and room temperature) [39]; (△), palygorskite (pH 6.0–8.0 and T = 295 K) [34].

5. Conclusions

The effect of pH upon removal of Cd^{2+} ions from aqueous solution using the microporous titanosilicate ETS-4 has been investigated in batch stirred tank experiments.

The results obtained show that Cd^{2+} removal increases with increasing pH. The amount of metal ion removed by ETS-4 is much higher at pH 6 than at pH 4, which is a very important result since the pH of industrial effluents and other wastewaters is around 6. Specifically, increments higher than 12.5 and 16 times were found under the experimental conditions studied. When pH is further increased till 8, the Cd^{2+} uptake is only slightly increased being imperceptible at equilibrium. Such results highlight the role that ETS-4 may play in future tertiary water treatments.

Results reveal the remarkable ion exchange capacity of ETS-4 and show that 12 h are sufficient to remove 99.6% of Cd^{2+} from an aqueous solution with initial concentration of 0.85×10^{-3} kg m^{-3} using 50.3×10^{-6} kg of titanosilicate at pH 6.

The equilibrium data at pH 6 were accurately represented by the Langmuir–Freundlich isotherm under the experimental conditions studied, with an AAD of only 1.67%. The amount of Cd^{2+} removed by ETS-4 at pH 6 clearly surmount results found in literature for the same titanosilicate at pH 4 and for different materials, such as dolomite (pH 5.0), clinoptilolite (pH 6.2), clarified sludge (pH 5.0), and palygoskite (pH 6.0–7.0). This result confirms the potential of ETS-4 as a decontaminant agent for wastewaters and aqueous effluents.

The kinetic of Cd^{2+} uptake by ETS-4 was studied using a Nernst–Planck based model, combining both film and intraparticle diffusion control, where the convective mass transfer coefficient and the self-diffusivities of Cd^{2+} and Na^{+} are the unique parameters. This model provided reasonable data representation, corresponding to AAD = 17.22%. The fitted diffusion coefficients of Cd^{2+} and Na^{+} were 4.548×10^{-19} and 5.246×10^{-18} m^2 s^{-1}, respectively, which evidence the higher mobility of sodium ions inside the particle and are consistent with data found in literature for ETS-4 and other microporous materials.

Acknowledgments

Patrícia F. Lito wishes to thank PhD grant provided by Fundação para a Ciência e Tecnologia (Portugal) (SFRH/BD/25580/2005). Authors acknowledge FEDER for financial support.

References

[1] B. Biskup, B. Subotic, Removal of heavy metal ions from solutions by means of zeolites: I. Thermodynamics of the exchange processes between cadmium ions from solution and sodium ions from zeolite, A. Sep. Sci. Technol. 33 (4) (1998) 449–466.
[2] V.J. Inglezakis, M.D. Loizidou, H.P. Grigoropoulou, Equilibrium and kinetic ion exchange studies of Pb^{2+}, Cr^{3+}, Fe^{3+} and Cu^{2+} on natural clinoptilolite, Water Res. 36 (11) (2002) 2784–2792.
[3] WISE – Water information system for water: http://ec.europa.eu/environment/water/water-dangersub/pri_substances.htm.
[4] Decreto-Lei n. 236/98, 01-08-1998: http://bdjur.almedina.net/item.php?field=node_id&value=702871.
[5] R. Petrus, J. Warchol, Ion exchange equilibrium between clinoptilolite and aqueous solutions of Na^{+}/Cu^{2+}, Na^{+}/Cd^{2+} and Na^{+}/Pb^{2+}, Microporous Mesoporous Mater. 61 (2008) 137–246.
[6] A. Dabrowski, Z. Hubicki, P. Podkoscielny, E. Robens, Selective removal of the heavy metal ions from waters and industrial wastewaters by ion-exchange method, Chemosphere 56 (2004) 91–106.
[7] M. Trgo, J. Peric, N.V. Medvidovic, Investigations of different kinetic models for zinc ions uptake by a natural zeolitic tuff, J. Environ. Manage. 79 (2006) 298–304.
[8] J.S. Watson, Separation Methods for Waste and Environmental Applications, Marcel Dekker, Inc., New York, 1999.
[9] B. Biskup, B. Subotic, Kinetic analysis of the exchange processes between sodium ions from zeolite A and cadmium, copper and nickel ions from solutions, Sep. Purif. Technol. 37 (2004) 17–31.
[10] M. Trgo, J. Peric, N.V. Medvidovic, A comparative study of ion exchange kinetics in zinc/lead-modified zeolite-clinoptilolite systems, J. Hazard. Mater. B 136 (2006) 938–945.
[11] J. Rocha, M.W. Anderson, Microporous titanosilicates and other novel mixed octahedral–tetrahedral framework oxides, Eur. J. Inorg. Chem. 2000 (5) (2000) 801–818.
[12] A.I. Bortun, L.N. Bortun, A. Clearfield, Evaluation of synthetic inorganic ion exchangers for cesium and strontium removal from contaminated groundwater and wastewater, Solvent Extr. Ion Exch. 15 (5) (1997) 909–929.
[13] J.G. Decaillon, Y. Andres, B.M. Mokili, J.C. Abbe, M. Tournoux, J. Patarin, Study of the ion exchange selectivity of layered titanosilicate $Na_3(Na,H)Ti_2O_2[Si_2O_6]22H_2O$, AM-4, for strontium, Solvent Extr, Ion Exch. 20 (2) (2002) 273–291.
[14] Y. Koudsi, A. Dyer, Sorption of 60Co on a synthetic titanosilicate analogue of the mineral penkvilksite-2O and antimonysilicate, J. Radioanal. Nucl. Chem. 247 (1) (2001) 209–219.
[15] C.B. Lopes, M. Otero, J. Coimbra, E. Pereira, J. Rocha, Z. Lin, A. Duarte, Removal of low concentration Hg^{2+} from natural waters by microporous and layered titanosilicates, Microporous Mesoporous Mater. 103 (1–3) (2007) 325–332.
[16] C.B. Lopes, P.F. Lito, M. Otero, Z. Lin, J. Rocha, C.M. Silva, E. Pereira, A. Duarte, Mercury removal with titanosilicate ETS-4: batch experiments and modelling, Microporous Mesoporous Mater. 115 (2008) 98–105.
[17] C.B. Lopes, M. Otero, Z. Lin, C.M. Silva, E. Pereira, J. Rocha, A. Duarte, Mercury removal from aqueous solution using ETS-4–kinetic and equilibrium study, Chem. Eng. J. 151 (2009) 247–254.
[18] T.R. Ferreira, C.B. Lopes, P.F. Lito, M. Otero, Z. Lin, J. Rocha, E. Pereira, C.M. Silva, A. Duarte, Cadmium (II) removal from aqueous solution using microporous titanosilicate ETS-4, Chem. Eng. J. 147 (2009) 173–179.
[19] K. Popa, C.C. Pavel, N. Bilba, A. Cecal, Purification of waste waters containing $^{60}Co^{2+}$, $^{115m}Cd^{2+}$ and $^{203}Hg^{2+}$ radioactive ions by ETS-4 titanosilicate, J. Radioanal. Nucl. Chem. 269 (1) (2006) 155–160.
[20] L. Lv, G. Tsoi, X.S. Zhao, Uptake equilibria and mechanisms of heavy metal ions on microporous titanosilicate ETS-10, Ind. Eng. Chem. Res. 43 (2004) 7900–7906.
[21] J.H. Choi, S.M. Kim, Y.J. Kwon, W.J. Kim, Adsorption behaviors of ETS-10 and its variant, ETAS-10 on the removal of heavy metals, Cu^{2+}, Co^{2+}, Mn^{2+} and Zn^{2+} from a waste water, Microporous Mesoporous Mater. 96 (2006) 157–167.
[22] F. Helfferich, Ion Exchange, Dover, NY, 1995.
[23] J.F. Rodrígez, J.L. Valverde, A.E. Rodrigues, Measurement of effective self-diffusion coefficients in a gel-type cation exchanger by the zero-length-column method, Ind. Eng. Chem. Res. 37 (1998) 2020–2028.
[24] J.L. Valverde, A. De Lucas, M. Carmona, M. González, J.F. Rodrígez, A generalized model for the measurement of effective diffusion coefficients of heterovalent ions in ion exchange by zero-length column method, Chem. Eng. Sci. 59 (2004) 71–79.
[25] S.M. Kuznicki, U.S. Patent 4,938,939, Assigned to Engelhard Corporation (1990).
[26] F.J. Holler, D.A. Skoog, S.R. Crounh, Principles of Instrumental Analysis, sixth edition, Thomson, Canada, 2007.
[27] W.E. Schiesser, The Numerical Method of Lines, Academic Press, USA, 1991.
[28] W.H. Lawton, E.A. Sylvestre, Elimination of linear parameters in nonlinear regression, Technometrics 13 (1971) 461–467.
[29] P.M. Armenante, D.J. Kirwan, Mass transfer to microparticles in agitated systems, Chem. Eng. Sci. 44 (1989) 2781–2796.
[30] M.A. Fernandez, G. Carta, Characterization of protein adsorption by composite silica-polyacrylamide gel anion exchangers. I. Equilibrium and mass transfer in agitated contactors, J. Chromatogr. A 746 (1996) 169–183.
[31] A. Bhattacharya, Predicting rates of dissolution of polydisperse solids in reactive media, Chem. Eng. Process. 46 (2007) 573–583.
[32] D.M. Ruthven, Principles of Adsorption and Adsorption Processes, John Wiley and Sons, USA, 1984.
[33] S.P. Mishra, V.K. Singh, D. Tiwari, Radiotracer technique in adsorption study: Part XVII. Removal behaviour of alkali metal (K- and Li-) titanates for Cd(II), Appl. Radiat. Isot. 49 (12) (1998) 1467–1475.
[34] S. Kocaoba, Comparison of amberlite IR 120 and dolomite's performances for removal of heavy metals, J. Hazard. Mater. 147 (2007) 488–496.
[35] A.M. El-Kamash, Evaluation of zeolite A for the sorptive removal of Cs^{+} and Sr^{2+} ions from aqueous solutions using batch and fixed bed column operations, J. Hazard. Mater. 151 (2008) 432–445.
[36] E.D. Camarinha, P.F. Lito, B.M. Antunes, M. Otero, Z. Lin, J. Rocha, E. Pereira, A.C. Duarte, C.M. Silva, Cadmium (II) removal from aqueous solution using microporous titanosilicate ETS-10, Chem. Eng. J. 155 (2009) 108–114.
[37] M. Sprynskyy, B. Buszewski, A.P. Terzyk, J. Namiesnik, Study of the selection mechanism of heavy metal (Pb^{2+}, Cu^{2+}, Ni^{2+}, and Cd^{2+}) adsorption on clinoptilolite, J. Colloid Interface Sci. 304 (2006) 21–28.
[38] T.K. Naiya, A.K. Bhattacharya, S.K. Das, Removal of Cd(II) from aqueous solutions using clarified sludge, J. Colloid Interface Sci. 325 (2008) 48–56.
[39] E. Álvarez-Ayuso, A. García-Sánchez, Removal of cadmium from solutions by palygorskite, J. Hazard. Mater. 147 (2007) 594–600.